Variational Quantum Algorithms in First Quantization

Jorge Gidi, Luciano Pereira, and Cristian Tabares

queen_of_fog
February 22, 2024

1 Project description

Quantum simulation in first quantization is a promising way to reduce the number of qubits required by standard quantum algorithms in second quantization. However, these algorithms need initial states with enough overlap with the actual ground state. In this project, we develop a pennylane-based module that implements a variational quantum eigensolver for quantum systems in first quantization. The method permits the preparation of the ground state of arbitrary Hamiltonians in terms of position and momentum.

In a fault-tolerant context, the proposed protocol could be used to prepare quantum states with high overlap with the actual ground state to be used as initial states for phase estimation algorithms (requiring fewer qubits than their second-quantized counterparts). But in a NISQ context, the shallow circuits can already find applications with current hardware. We show the workflow of our module studying quantum systems such as single and coupled quantum harmonic oscillators (Secs. 4.1 and 4.2) and atoms and molecules of hydrogen (Secs. 4.3 and 4.4), besides a further application in quantum cryptography (Sec. 4.5). The codes are available in Github [1] and in the files attached to the project.

We submit our project to the following challenges:

- **The sound of silence**: The protocol reduces the number of qubits and circuits compared with the second quantization approach. Moreover, we implement a semiclassical Fourier Transform to reduce the negative impact of the controlled operations in a noisy context and enable the use of circuit cutting with the Fourier transform.
- **Preparing for battle**: The protocol permits preparing initial quantum states for other algorithms. We show two examples: the preparation of states with high overlap with the ground state for quantum chemistry, and the preparation of elliptic curves for quantum cryptography.
- **Bridging the gap**: Including penalization in the optimization process and imposing symmetric or antisymmetric conditions on the variational circuit, the protocol iteratively finds the four lowest energy eigenstates of the hydrogen atom. We also use circuit symmetry without penalization to find the ground state and excited state of the hydrogen molecule.

2 Motivation

The development of quantum computing, both in terms of algorithms and hardware, has recently reached a point of advantage over classical computers for certain problems: the so-called quantum advantage. The natural next step after this milestone is to look for a *practical quantum advantage*, that is, a quantum computer's advantage over a classical one in a task of practical interest [2]. Among the possible realms where a practical quantum advantage could be found, quantum simulation stretches back to Feynman's original proposal [3], and was soon highlighted as one of the most promising applications of quantum computers [4, 5].

Intuitively, this advantage arises from the exponential amount of resources needed to store a quantum state in a classical computer. Hence, although thousands of qubits and millions of quantum gates would be needed to find an advantage in other applications (such as factoring large

numbers), a few tens of qubits and thousand operations may be beyond what is currently classically tractable when simulating quantum systems. On top of this, the simulation of strongly correlated fermionic quantum systems is a task of enormous importance: it could be used to develop quantum chemistry or materials science further.

The problem we aim to solve then is the understanding of the Hamiltonian:

$$\hat{H}_{\mathrm{f}} = \sum_{j=1}^{N} \hat{H}_1(\hat{\boldsymbol{r}}_j) + \frac{1}{2} \sum_{i \neq j=1}^{N} \hat{V}_c(\hat{\boldsymbol{r}}_i, \hat{\boldsymbol{r}}_j)\,, \tag{1}$$

where bold letters indicate three-dimensional vectors. Here, $\hat{H}_1(\hat{\boldsymbol{r}}_j)$ is labeled as the single-electron part of the Hamiltonian and we include a pair-wise interaction between the fermions, $\hat{V}_c(\mathbf{r}_i, \mathbf{r}_j)$. To solve the Hamiltonian in Eq. (1), most of the quantum-computing algorithms for chemistry and materials science use second-quantized operators. The general recipe to do this needs a set of basis functions (typically single-particle states), $\mathcal{B} = \{|\phi_i\rangle\}$ [6]. This basis set is used to map the problem in real-space to the occupation-number representation defining the field operators:

$$\hat{\Psi}(\boldsymbol{r}) = \sum_i \phi_i(\boldsymbol{r}) \hat{c}_i\,, \tag{2a}$$

$$\hat{\Psi}^\dagger(\boldsymbol{r}) = \sum_i \phi_i^*(\boldsymbol{r}) \hat{c}_i^\dagger\,, \tag{2b}$$

that can be used to write the Hamiltonian in Eq. (1) in the following form:

$$\hat{H}_{\mathrm{f}} = \int d\boldsymbol{r} \hat{\Psi}^\dagger(\boldsymbol{r}) \hat{H}_1(\boldsymbol{r}) \hat{\Psi}(\boldsymbol{r}) + \frac{1}{2} \iint d\boldsymbol{r} d\boldsymbol{r}' \hat{\Psi}^\dagger(\boldsymbol{r}) \hat{\Psi}^\dagger(\boldsymbol{r}') \hat{V}_c(\boldsymbol{r}, \boldsymbol{r}') \hat{\Psi}(\boldsymbol{r}') \hat{\Psi}(\boldsymbol{r})\,. \tag{3}$$

If the basis of the function $\mathcal{B}$ was complete (i.e., infinite-dimensional), then the mapping between Eq. (1) and Eq. (3) would be exact. However, and this is the elephant in the room of this approach, in practical applications *the basis set is finite-dimensional, and the mapping to the second-quantized Hamiltonian is inexact.* This means that most of the existing methods for simulating quantum chemistry and quantum materials with this approach become impractical as they are scaled towards the continuum limit because *the number of qubits needed to retain a given accuracy scales linearly with the number of basis functions.*

A possible workaround to this problem dates back to Kassal *et al.* [7], where they introduced a proposal to perform first quantized chemistry simulations and avoid the mapping error. This technique was originally developed by Zalka [8] and Wiesner [9] and encodes the wavefunction $|\Psi\rangle$ in a register of N qubits defining a discretized position basis of $n = 2^N$ points. For a single particle wavefunction, this reads:

$$|\Psi\rangle = \sum_{x=0}^{2^N-1} \psi_x |x\rangle = \psi_0 |0 \ldots 00\rangle + \psi_1 |0 \ldots 01\rangle + \psi_2 |0 \ldots 10\rangle + \cdots + \psi_{2^N-1} |1 \ldots 11\rangle\,. \tag{4}$$

The main advantages of this method are two: first, the number of qubits needed to represent the state only scales logarithmically with the number of orbitals instead of linearly (as would be the case of second-quantized approaches). Second, since there is no need to use the Born-Oppenheimer approximation to decouple the motion of the nuclei, this approach can be easily adapted to cases where the entanglement between the electronic and the nuclear degrees of freedom is not negligible.

Besides these pioneering results, quantum simulation in first quantization has recently received the community's attention. Several pioneering works highlight its advantages against its second-quantized counterpart when all the constant factors in the implementation are rigorously estimated [10, 11]. These promising results generated interest in the community and led to proposals studying quantum systems of practical interests, such as batteries [12, 13].

However, although the algorithms described above offer an advantage in terms of the number of qubits needed compared to their second-quantized counterparts, their resource demands are still far beyond what will be achievable in the next years. Furthermore, these fault-tolerant algorithms are based on Quantum Phase Estimation, which is known to need an initial state with enough

overlap with the actual ground state to provide a good result. In quantum chemistry and quantum materials problems, the Hartree-Fock state is typically used, but this is known to be not a good option for strongly correlated systems [14], which are precisely the target application of quantum algorithms. Although previous works have studied the initial state preparation task in detail for second-quantized algorithms [15], an explicit and good heuristic is currently missing to prepare initial states in first-quantized quantum algorithms.

Although Variational Quantum Algorithms suffer from different caveats and may not be trainable in some cases [16] (due to barren plateaus and local minima), they are still an appropriate heuristic tool that can be used as a first step in quantum algorithms [17]. Therefore, what we propose in this project is a state-preparation algorithm based on a first-quantized version of the Variational Quantum Eigensolver, following the original spirit of Ref. [18]. The protocol evaluates the expected value of the Hamiltonian by measuring it in two bases, the computational (in real space) and the Fourier one (in momentum space), highly reducing the number of circuits compared with the second-quantization proposal, which typically scales as $\mathcal{O}(N^4)$, with N the number of qubits [19]. This algorithm could be used as a first step in the algorithms described in Refs. [10, 11, 12, 13], where the VQE in first quantization offers an initial state with a greater overlap with the real ground state than a simple Hartree-Fock approximation. This would improve the performance of these algorithms and ultimately lead to an advantage in terms of qubits when comparing the corresponding simulation using quantum algorithms targeted to a second-quantized Hamiltonian.

3 Methods

Our objective is the solution of the Schrodinger equation, $\hat{H}\,|\Psi\rangle = E\,|\Psi\rangle$. For simplicity, we consider a single particle in one dimension, although this can be easily generalized, increasing the number of quantum registers (as we will do later). Projected to real space, the equation reads:

$$H(x,p)\psi(x) = E\psi(x)\,. \tag{5}$$

Since the momentum operator in this representation involves derivatives of x, solving the Schrodinger equation implies the solution of an ODE. However, since the Hamiltonian is bounded from below with a minimum value of E, $E_{\min}$, it is possible to solve Eq. (5) using a variational method. The quantum algorithm that we propose, inspired by Ref. [18], parametrizes the state $|\Psi\rangle = |\Psi\,(\boldsymbol{\theta})\rangle$ with a vector $\boldsymbol{\theta}$ of parameters and goes as follows:

1. The function $\psi(x)$ is discretized and encoded in an N qubit register, $|\Psi\rangle = \sum_{x=0}^{2^N-1}\psi_x\,|x\rangle$. With this encoding, the measurement of the qubits in the computational basis accounts for the measurement of the $\hat{X}$ operator, so any function $\langle f(x)\rangle_{\boldsymbol{\theta}} = \langle\Psi\,(\boldsymbol{\theta})\,|f(\hat{X})|\Psi\,(\boldsymbol{\theta})\rangle$ can be evaluated over this register with classical post-processing.

2. The Quantum Fourier Transform (QFT), denoted as $\mathcal{F}$, transforms $|\Psi\rangle$ from the real space encoding described above to encoding in momentum space. The measurement of the qubits in the computational basis now allows the measurement of the $\hat{P}$ operator, so it is possible to compute the value of any function of the momentum as $\langle g(p)\rangle_{\boldsymbol{\theta}} = \langle\Psi\,(\boldsymbol{\theta})\,|\mathcal{F}^{-1}g(\hat{P})\mathcal{F}|\Psi\,(\boldsymbol{\theta})\rangle$.

3. Combining the results above it is possible to obtain the expectation value over the parametrized state of any possible Hamiltonian as $\langle H(x,p)\rangle_{\boldsymbol{\theta}} = \langle f(x)\rangle_{\boldsymbol{\theta}} + \langle g(p)\rangle_{\boldsymbol{\theta}}$. This expectation value can be minimized by tuning the parameter $\boldsymbol{\theta}$. This performs a *Variational Quantum Eigensolver in first quantization*, and (if converged) leads to an encoding of the ground state of $H(x,p)$ in the parametrized state $|\Psi(\boldsymbol{\theta})\rangle$.

4. The parameters $\boldsymbol{\theta}_{\text{opt}}$ encoding the ground state can be then used to prepare a good initial state for Quantum Phase Estimation or include the projection over them a penalty in the cost function to calculated excited eigenstates (following Ref. [20]).

Regarding the second step, let us note that since the QFT is applied at the end of the circuit (right before the measurements), it is not necessary to implement the full quantum-mechanical operator. Instead, the semiclassical Fourier transform [21, 22, 23, 24] (also known as Kitaev's

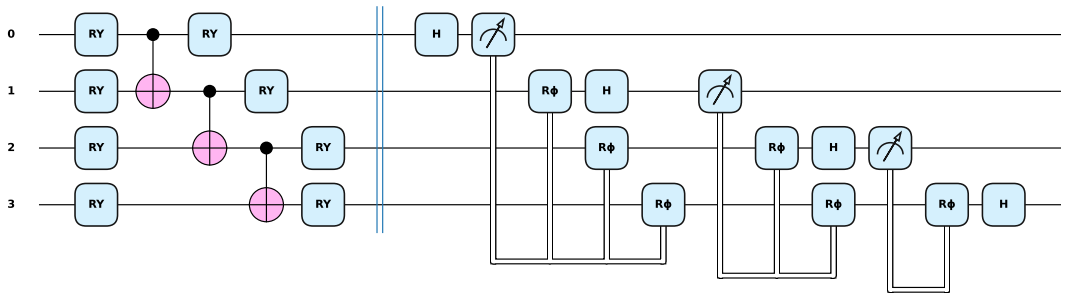

Figure 1: Circuit for one layer of the Hardware Efficient Ansatz used in this project followed by the semiclassical Fourier transform (shown here for $N = 4$ qubits). We use single qubit rotations around the y axis and CNOT gates to entangle as our ansatz, and implement the QFT with classical controls instead of quantum ones following Kitaev's approach [25].

QFT [25]) can be performed. This modification of the regular QFT implies measuring the qubits along the register in descending order, adding a classically controlled rotation before each measurement that depends on the results obtained in the previous qubits, as shown Fig.1. Such a procedure offers a twofold advantage: on the one hand, it does not need to add any entangling two-qubit gate to implement the QFT. Since these gates generate the biggest errors, this is an advantage in noisy devices. But even in the case of fault-tolerant devices, implementing the semiclassical QFT instead of the full QFT allows the use of circuit-cutting techniques (otherwise impossible due to the high connectivity needed by the QFT).

In the notebook "`1_Quadrature_Operators.ipynb`", located in the folder "`tutorials`" of the final project attached, we demonstrate our implementation of a framework based on Pennylane to study quantum algorithms in first quantization. Our code maps a quantum register to its real space representation according to Eq. (4). It also allows the transformation of this representation to momentum space and the implementation general operators $\hat{Q} = f(\hat{X}) + g(\hat{P})$. We note that the classes we develop here are completely general, can include several particles, and will be the basis of all the results shown in the next section.

4 Results

4.1 The quantum harmonic oscillator

The demonstration of the results discussed in this subsection is shown in "`tutorials/2_Harmonic_Oscillator.ipynb`" **and** "`tutorials/7_Harmonic_Oscillator_with_semi_classical_QFT.ipynb`"

As a first test of our algorithm, we consider a simple quantum harmonic oscillator. Its Hamiltonian reads:

$$\hat{H} = \frac{\hat{P}^2}{2} + \frac{\hat{X}^2}{2}\,, \tag{6}$$

where $\hat{P}$ and $\hat{X}$ are the momentum and position operators, respectively. To find its ground state, we follow the algorithm described in Sec. 3. We define a grid going from $x_{\min} = -5$ to $x_{\max} = 5$ and encode it using $N = 6$ qubits. We use a Hardware Efficient Ansatz (HEA) [26] with $D = 6$ layers (we found that $D = N$ is needed to obtain accurate results with HEA circuits). The circuit for one layer is shown in Fig. 1 before the barrier (after the barrier, we plot the circuit for the semiclassical Fourier Transform that we also implement; the circuit for the conventional Quantum Fourier Transform would use quantum controls instead of classical ones, following any textbook implementation).

Regarding the results, in Fig. 2(a) we show the loss function values as the optimization is performed. Although the energy of the ground state of a quantum harmonic oscillator in 1D is

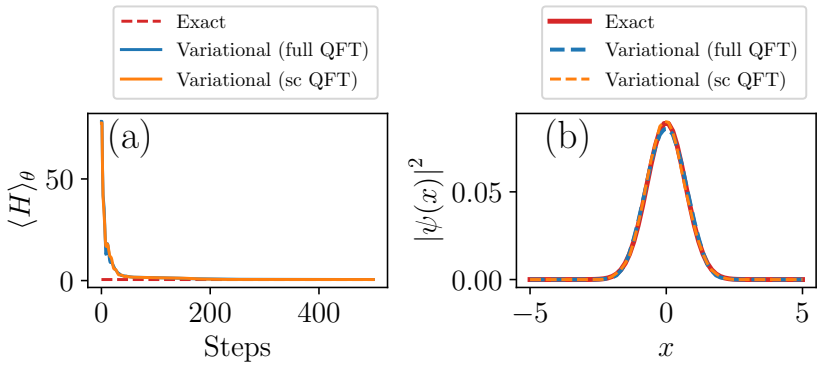

Figure 2: (a) Value of the loss function for the different optimization steps for the quantum harmonic oscillator described in Eq. (6). In both cases it converges to the ground state energy $E_{\text{gs}} = 1/2$ with an error smaller than 10^{-3}. (b) The probability density in real space for the variational approximations of the ground state of the harmonic oscillator using a full QFT and its semiclassical version, compared with the exact one (obtained as the lowest energy eigenstate of the operator $\hat{H}(\hat{X}, \hat{P})$, which can be calculated numerically).

known to be $E_{\text{gs}} = 1/2$, we also check our encoding, calculating it from the diagonalization of $\hat{H}(\hat{X}, \hat{P})$ and indeed obtain the same result. Remarkably, we also note that both the full Quantum Fourier Transform and its semiclassical version provide accurate results and are able to generate the ground state. This is even more noticeable when looking at Fig. 2(b), which shows the probability density $|\psi(x)|^2$ of the encoded wavefunction. It is obtained from the optimized variational state, measuring in the computational basis and relating each element of possible result to a discretized element of real space, according to Eq. 4.

In summary, this section shows that it is possible to use the algorithm described in Sec. 3 to accurately solve the Schrodinger equation and obtain the ground state of a simple system, in this case, a quantum harmonic oscillator. This benchmarks our implementation of quantum algorithms in first quantization. In the following, we will add different layers of complexity to this problem to obtain physical insights about more complicated systems.

4.2 Coupled quantum harmonic oscillators

The demonstration of the results discussed in this subsection is shown in "`tutorials/3_Coupled_Harmonic_Oscillators.ipynb`"

The single-particle system studied above is a proper first benchmark. Still, the framework that we have implemented is much more general and can be used to study many-body systems. Hence, as an extension of the previous example, we now study two coupled harmonic oscillators. Their Hamiltonian (neglecting overall constant factors) reads:

$$\hat{H} = \hat{P}_1^2 + \hat{X}_1^2 + \hat{P}_2^2 + \hat{X}_1^2 - \frac{1}{2}\left(\hat{X}_1 - \hat{X}_2\right)^2 , \tag{7}$$

where $\hat{P}_i$ and $\hat{X}_i$ are respectively the momentum and position operators for the $i-$th particle. Note that we introduce an interaction term $\hat{H}_{\text{int}} = -\left(\hat{X}_1 - \hat{X}_2\right)^2/2$ that favors the delocalization of the individual oscillators (due to the negative sign), so it will compete with the localization generated by the single-particle terms.

Furthermore, note that the Hamiltonian is invariant under the exchange of particles. Hence, once the two particles are mapped to a common quantum register, the wavefunction will be symmetric around the origin of this register. We encode this in the ansatz, forcing it to be symmetric, using the circuit shown in Fig. 3. Moreover, we encode the total wavefunction using $2N$ qubits instead of N (half of them for each particle) and take $N = D/2-1 = 4$. The final result is shown in

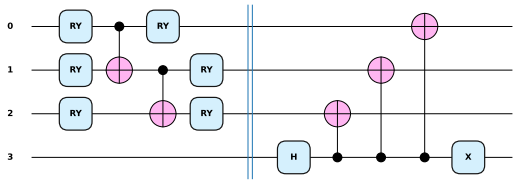

Figure 3: Circuit for one layer of the symmetrized version of the Hardware Efficient Ansatz used in this project. We use a regular HEA (c.f. Fig. 1) over the first $N-1$ qubits and use the last one to symmetrize the function. Implementing a Z gate over the last qubit instead of the shown X gate would antisymmetrize the final function.

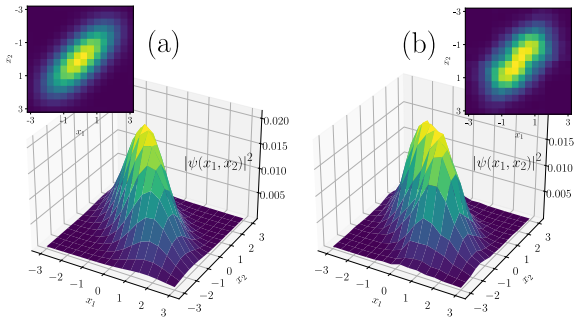

Figure 4: Probability density in real space, $|\psi(x_1, x_2)|^2$, of the ground state of the coupled quantum harmonic oscillators described by the Hamiltonian in Eq. (7). The negative coupling favors the delocalization of the individual particles. (a) Exact wavefunction, obtained diagonalizing the operator $\hat{H}(\hat{X}_1, \hat{P}_1, \hat{X}_2, \hat{P}_2)$. (b) Variational wavefunction obtained after the optimization.

Fig. 4, with Fig. 4(a) showing the exact ground state and Fig. 4(b) the variational approximation. As expected, the negative coupling between the oscillators induces a delocalization of each of the particles, and remarkably, the variational ansatz is able to capture this.

4.3 Towards quantum chemistry: eigenstates of an hydrogen atom

The demonstration of the results discussed in this subsection is shown in "`tutorials/4_H_Atom.ipynb`"

In the previous examples, we dealt with quantum harmonic oscillators, but our first-quantization framework supports completely general operators. Thus, and following our final goal (the solution of many-body electronic Hamiltonians), we now solve the unidimensional Hydrogen atom. Once the dynamics of the center of mass are decoupled from the relative movement, and neglecting the former since they only introduce a global energy shift, the Hamiltonian for the Hydrogen atom reads:

$$\hat{H} = \frac{1}{2}\left(\hat{P}^2 - \frac{1}{|\hat{X}|}\right), \tag{8}$$

where the first term accounts for the kinetic energy, meanwhile the second one is the interaction between the electron and the nucleus according to Coulomb's law.

This unidimensional Hydrogen atom is an interesting system by itself, with open questions regarding its analytical eigenspectrum [27]. However, avoiding singularities near to $x = 0$, this system behaves similarly to its three-dimensional counterpart, including an *approximate* scaling of its eigenenergies as $E_n \sim -E_0/n^2$ (which is exact in the case of three dimensions and can be traced back to the Rydberg formula in atomic physics). Although the algorithms used in the previous sections were only used to calculate ground states, they can be easily extended to the full eigenspectrum [20]. The idea is to exploit the fact that the eigenstates of a Hamiltonian are orthogonal. Thus, we run the algorithm described in Sec. 3 once to obtain the ground state of Eq. (8), $|\Psi_1\rangle$. This state is shown in Fig. 5 (panel $n = 1$), where it can be seen that it perfectly

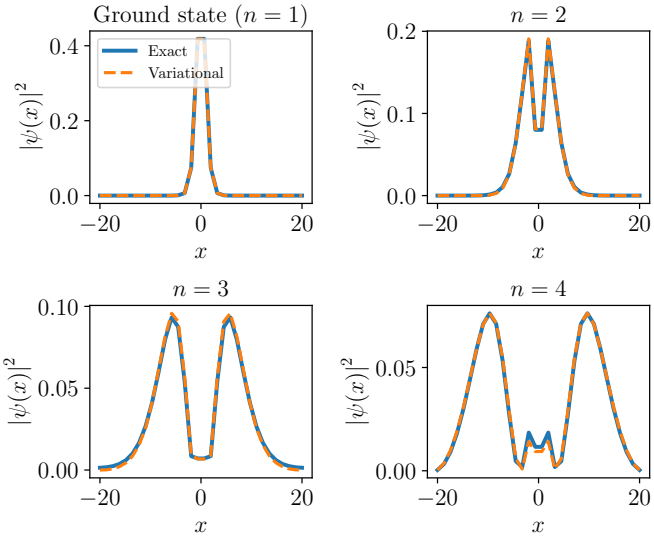

Figure 5: Probability density in real space evaluated over the ground state ($n = 1$) and the first three excited states ($n = 2$, $n = 3$ and $n = 4$ in ascending energy) of the Hamiltonian in Eq. (8), corresponding to a one-dimensional Hydrogen atom.

matches the exact ground state of the system (discretized over the chosen lattice). Then, the circuit is re-optimized using as a cost function the expectation value of the modified Hamiltonian $\hat{H}' = \hat{H} + b\,|\Psi_1\rangle\langle\Psi_1|$, with b a real number bigger than the difference between the first and the second eigenenergy. This new term in $\hat{H}'$ penalizes in energies only the state $|\Psi_1\rangle$, so the ground state of $\hat{H}'$ is the first excited state of $\hat{H}$. This is shown in the panel $n = 2$ of Fig. 5, again matching the first excited state of the full Hamiltonian $\hat{H}$ obtained with exact diagonalization. This procedure can be iterated, including now an extra penalty term over the first excited state, so the ground state of the Hamiltonian $\hat{H}'' = \hat{H} + b\,(|\Psi_1\rangle\langle\Psi_1| + |\Psi_2\rangle\langle\Psi_2|)$ is the next excited state, labeled with $n = 3$ in Fig. 5. Although we stop the calculation at $n = 4$, this procedure can be iterated to obtain virtually as many excited states as desired.

Furthermore, as described above, this one-dimensional hydrogen atom has an approximate scaling of its eigenenergies as $E_n \sim -E_0/n^2$. To check whether our variational quantum algorithm eigensolver in first quantization is able to capture this behavior, in Fig. 6, we plot the logarithm of the variational energies against the logarithm of the quantum number n for the lowest four eigenstates shown in Fig. 5. A linear fit to this data yields a slope of ~ -2.05, in accordance with the expected behavior (a scaling of $1/n^2$ plus a correction term to account for the one-dimensionality). Remarkably, this result shows that the variational quantum simulators in first quantization proposed in this project can capture non-trivial results in atomic physics (the Rydberg law) without encoding any Hamiltonian and performing the calculation directly in real space with a quantum computer.

Finally, regarding the technical details, let us note that the results described in this section use a ZGR ansatz [18] instead of the HEA. This is known to be a good choice in a general case since this ansatz can encode arbitrary probability distributions. Its circuit is shown in Fig. 7, and we also include the protocol described in Fig. 3 to symmetrize or antisymmetrize it, following the known parity of the eigenstates of the Hydrogen atom.

4.4 A many-body electronic system: the H_2 molecule

The demonstration of the results discussed in this subsection is shown in "`tutorials/5_H2_Molecule.ipynb`"

The last physical system we study already shows the capabilities of quantum simulation in first quantization when comparing it to the typical algorithms in second quantization. We calculate the

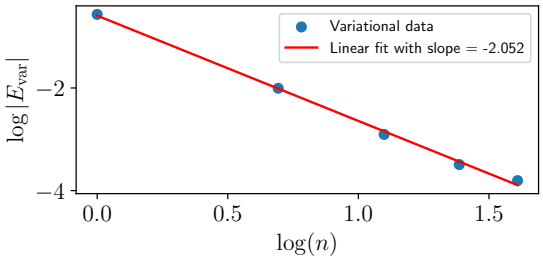

Figure 6: Logarithm of the variational energies obtained for the lowest four eigenstates of the Hydrogen atom shown in Fig. 5 against the logarithm of their corresponding quantum number. The linear fit yields the expected approximate scaling following Rydberg's law, $E_n \sim -E_0/n^2$.

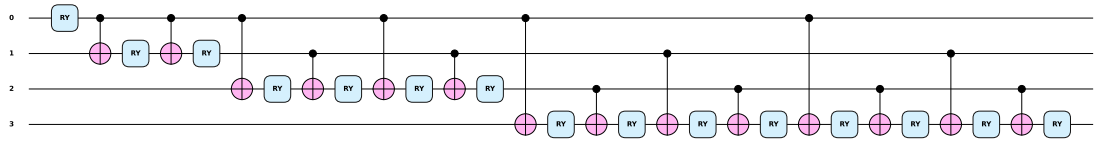

Figure 7: Circuit for the ZGR ansatz.

ground state and the first excited state (to compute the spectral gap) of the following Hamiltonian:

$$\hat{H} = \hat{H}_{\text{kin}} + \hat{H}_{\text{el-nuc}} + \hat{H}_{\text{el-el}} \tag{9a}$$

$$\hat{H}_{\text{kin}} = \hat{P}_1^2 + \hat{P}_2^2 \tag{9b}$$

$$\hat{H}_{\text{el-nuc}} = -\frac{1}{|\hat{X}_1 - R|} - \frac{1}{|\hat{X}_1 + R|} - \frac{1}{|\hat{X}_2 - R|} - \frac{1}{|\hat{X}_2 + R|} \tag{9c}$$

$$\hat{H}_{\text{el-el}} = +\frac{1}{|\hat{X}_1 - \hat{X}_2|}\,, \tag{9d}$$

where $\hat{X}_i$ and $\hat{P}_i$ are the position and momentum operators for the $i-$th particle. Physically, this Hamiltonian represents a simple description of an H_2 molecule under the Born-Oppenheimer approximation: two fixed nuclei located at a distance $2R$ interacting with two electrons, whose state is the one we are interested in. $\hat{H}$ includes then the kinetic energy of the electrons $\hat{H}_{\text{kin}}$, the interaction between them and the two nucleus $\hat{H}_{\text{el-nuc}}$ and also the electron-electron interaction $\hat{H}_{\text{el-el}}$.

4.4.1 Antiferromagnetic interaction

The Hamiltonian in Eq. (9a) is the simplest model for quantum chemistry and quantum materials. In particular, if the atoms are located at an infinite distance, they do not interact, and their ground state is a degenerate product state. However, if they are now brought together (decreasing R from infinity to a big but finite value), they start interacting antiferromagnetically, and the degeneracy of the ground state is broken, leading to a symmetric singlet state of lower energy and an antisymmetric triplet state of slightly more energy [28]. In both cases, the electrons are still localized around their corresponding nucleus.

The antiferromagnetic ground and first excited states can be computed easily with the quantum algorithm described in this project. We encode the total wavefunction in $2N$ qubits (half of them for each electron) and use a HEA with $N = D/2 - 1 = 4$. We anticipate that the ZGR ansatz used in Sec. 4.3 would lead to better results, but the running time of the simulations became unfeasible for this project. However, since the singlet and the triplet states are very close in energy but have opposite parity, we compute them using the symmetrized (or antisymmetrized) version of the HEA shown in Fig. 3. We note that this is a very different and powerful approach to the calculation

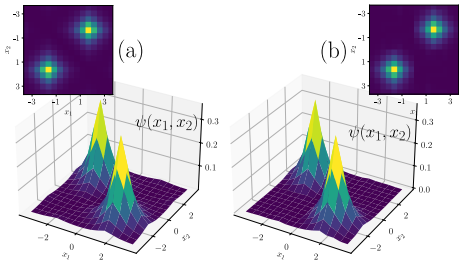

Figure 8: Wavefunction in real space, $\psi(x_1, x_2)$, of the singlet (symmetric) state of an H_2 molecule described by the Hamiltonian (9a) for $R = 1.75$. In this case, the molecules interact antiferromagnetically and the singlet state is the ground state. (a) Exact wavefunction, obtained from exact diagonalization of the operator $\hat{H}$. (b) Variational wavefunction obtained after the optimization.

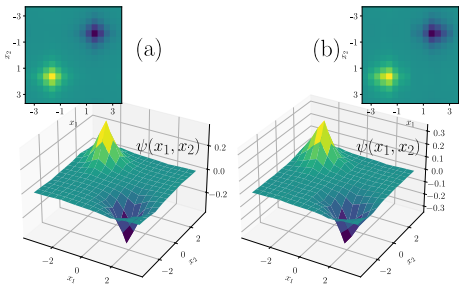

Figure 9: Wavefunction in real space, $\psi(x_1, x_2)$, of the triplet (antisymmetric) state of an H_2 molecule described by the Hamiltonian (9a) for $R = 1.75$. In this case, the molecules interact antiferromagnetically and the triplet state is the first excited state. (a) Exact wavefunction, obtained from exact diagonalization of the operator $\hat{H}$. (b) Variational wavefunction obtained after the optimization.

of ground and excited states: instead of including a penalty in the cost function, as we did in Sec. 4.3, we now design the circuit in such a way that the output state is *forced* to have the desired symmetry.

The results for the symmetric singlet state and the antisymmetric triplet state are shown in Figs. 8 and 9, respectively, where we solve the Hamiltonian (9a) for $R = 1.75$. Our quantum algorithm is able to capture these physics easily, producing approximations of the singlet [Fig. 8(b)] and triplet [Fig. 9(b)] states that almost match the ones obtained from exact diagonalization [Figs. 8(a) and 9(a), respectively]. Finally, let us note that by measuring the Hamiltonian over these states, it is possible to obtain the energy gap ΔE between the symmetric ground state and the antisymmetric first excited state. In this case, we find that:

$$\Delta E = E_{\text{ex}} - E_{\text{gs}} \approx 0.1915\,. \tag{10}$$

In this simple toy model, however, we are making two different approximations: first, we are not including the spin degree of freedom of the electrons. And second, we are not imposing the global antisymmetry of the wavefunction under electron exchange. Although both can be included easily, forcing them in the quantum circuit [5], in a real system, these two phenomena compensate. The symmetric/antisymmetric wavefunction in real space is accompanied by an antisymmetric/symmetric wavefunction in spin space, so Fermi statistics are maintained. This situation allows the physical interpretation of our results exactly as one would interpret the ones obtained with spinful electrons: the singlet state, symmetric in real space, needs to have opposite spins for each electron. This means that electrons can then hop from one atom to the other while the original electron is still there, reducing their kinetic energy and obtaining a lower energy state. Nevertheless, this is not allowed for the (antisymmetric in real space) triplet states, which need to be symmetric in spin space and, therefore, have parallel spins. This means that this virtual hopping is not allowed, the electrons cannot hybridize, and the energy of the triplet is greater than the energy of the singlet. Remarkably, **our quantum algorithm is able to reproduce the physics of such antiferromagnet from its first principles Hamiltonian, providing physical insights into the real system**.

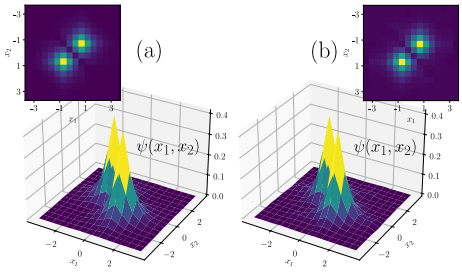

Figure 10: Wavefunction in real space, $\psi(x_1, x_2)$, of the symmetric (ground) state of an H_2 molecule described by the Hamiltonian (9a) for $R = 0.6$. In this case, there is a competing order between the antiferromagnetic and the ferromagnetic interactions, but the symmetric state is still the ground state. (a) Exact wavefunction, obtained from exact diagonalization of the operator $\hat{H}$. (b) Variational wavefunction obtained after the optimization.

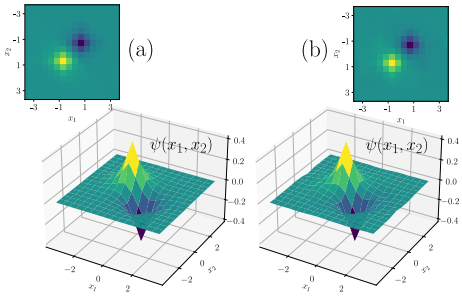

Figure 11: Wavefunction in real space, $\psi(x_1, x_2)$, of the antisymmetric (first excited) state of an H_2 molecule described by the Hamiltonian (9a) for $R = 0.6$. In this case, there is a competing order between the antiferromagnetic and the ferromagnetic interactions. Although the antisymmetric state is still the excited state, the energy gap in this case [c.f. Eq. (11)] is smaller than in the more antiferromagnetic case [c.f. Eq. (10)]. (a) Exact wavefunction, obtained from exact diagonalization of the operator $\hat{H}$. (b) Variational wavefunction obtained after the optimization.

4.4.2 Competing order between the antiferromagnetic and the ferromagnetic interaction

If R keeps decreasing until the atoms are close together, their single-particle wavefunctions overlap. Physically, this means that electrons start delocalizing, and the previous antiferromagnetic interaction now competes with a new ferromagnetic one. In terms of spins, the antiparallel configuration found in the section above now competes with a parallel spin term in the ground state (corresponding to a ferromagnet). Hence, an antisymmetric real space wavefunction would be a more stable configuration than in the fully antiferromagnetic case to keep the total antisymmetry of the wavefunction. In other words, the energy gap calculated in Eq. (10) is smaller if R is decreased.

To demonstrate that our quantum algorithm can also capture this physics, now we solve the Hamiltonian (9a) for $R = 0.6$. The results are shown in Figs. 10 and 11, for the symmetric and the antisymmetric wavefunctions, respectively. The quantum algorithm captures the hybridization and delocalization of the electrons in this case [Figs. 10(b) and 11(b)], matching the wavefunctions obtained with exact diagonalization [Figs. 10(a) and 11(a)]. Regarding the energy gap, now it reads:

$$\Delta E = E_{\text{ex}} - E_{\text{gs}} \approx 0.0853\,, \tag{11}$$

smaller than the one obtained in the previous section [Eq. (10)] for the more antiferromagnetic case. This, in summary, means that **our quantum algorithm can also capture these competing interactions, reproducing their physics from its first principles Hamiltonian**. Finally, let us note that, for completeness, the tutorial "`5_H2_Molecule.ipynb`" that discusses these results considers the case of a fully ferromagnetic molecule, where the parity of the ground state and the excited state get exchanged.

4.5 Preparing interesting wavefunctions: elliptic curves

The demonstration of the results discussed in this subsection is shown in "`tutorials/6_Elliptic_curves.ipynb`"

One of the applications of the variational framework for first quantization systems developed in this project is the preparation of target eigenstates of a given Hamiltonian. This task is important for quantum machine learning, where the data has to be embedded in a quantum circuit to perform the computation, or quantum chemistry, where a state with high overlap with the ground state is required. However, another interesting application is the preparation of elliptic curves [29], which are defined as a set of points $(x, y) \in \mathbb{R}^2$ that satisfy the equation,

$$y^2 = ax^x + bx + c, \tag{12}$$

with some $a, b, c \neq 0$. Cryptography based on elliptic curves is one of the standard protocols for cybersecurity nowadays, so loading elliptic curves in quantum computers could be used to break their security with the Shor algorithm.

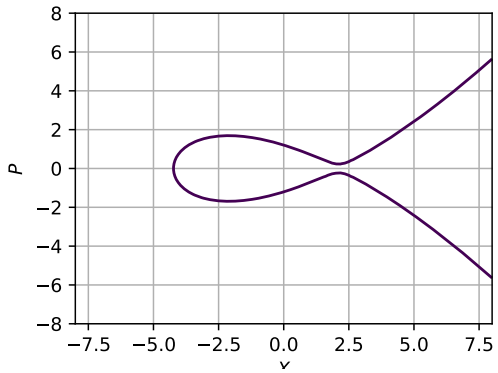

Figure 12: Elliptic curve with $a = 0.075$, $b = -1$, and $c = 1.475131$.

The elliptic curves can be identified as the classical trajectories in the phase space of a system described by the following classical Hamiltonian:

$$h(x, p) = \frac{1}{2m}p^2 - ax^3 - bx\,, \tag{13}$$

where we make the identification $h(x, p) = c$. Replacing the classical variables x and p with the quantum operators $\hat{X}$ and $\hat{P}$, we have the quantum version of this Hamiltonian,

$$\hat{H} = \frac{1}{2m}\hat{P}^2 - a\hat{X}^3 - b\hat{X}, \tag{14}$$

with $c = \langle\hat{H}\rangle$. Each eigenvector $|\psi_j\rangle$ of $\hat{H}$ corresponds to the quantum representation of the elliptic curve with $c_j = \langle\psi_j|\hat{H}|\psi_j\rangle$. Moreover, the positive part of the Wigner function [30] of $|\psi_j\rangle$ is concentrated over the classical trajectory of the elliptic curve.

We can prepare an eigenstate $|\psi_j\rangle$ of $\hat{H}$ with Variational Quantum Eigensolver in first quantization developed in this project. Our target is the elliptic curve with $a = 0.075$, $b = -1$, $c = 1.475131$, shown in Fig. 12. The eigenstate corresponding to these parameters can be found minimizing the objective function

$$f(\theta) = \Big(c_j - \langle\psi(\boldsymbol{\theta})|\hat{H}|\psi(\boldsymbol{\theta})\rangle\Big)^2. \tag{15}$$

The execution of this optimization, which can be found in the notebook "`6_Elliptic_curves.ipynb`", delivers a quantum state whose Wigner Function is shown in Fig 13. As was expected, it is concentrated around the classical trajectory of the elliptic curve.

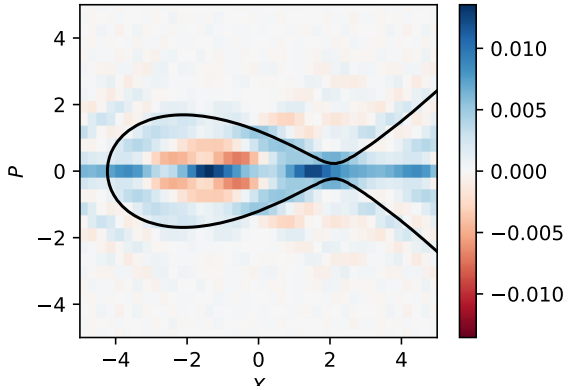

Figure 13: The Wigner function is associated with the ground state estimated by the variational algorithms for first quantization systems (color plot). The positive part of this Wigner is concentrated over the classical trajectory of the elliptic curve (black).

5 Outlook

In this project, we have developed a framework that can be used to study quantum systems in first quantization using quantum computers. Furthermore, we have implemented a complete module based on Pennylane to further encourage the community to look for other applications of these ideas. We think the results outlined in this project may serve as a bridge to connect large-scale fault-tolerant quantum algorithms in first quantization with the hardware that will be developed in the next few years.

Our project has several future avenues. The first is an in-depth study of different variational ansatz to increase the convergence rate of the simulations. In [31], it has been proposed to carry out a classical pre-training over a quantum circuit representing a matrix product state (MPS). This MPS is later used as an initial condition for the variation search by embedding its circuit in a larger one with more parameters, increasing its expressivity. The second avenue is the usage of classical Fourier extrapolation to increase the accuracy of the solution [18]. This effectively reduces the number of qubits required by the quantum algorithm since we can always improve the solution with only classical postprocessing. The third option is implementing a circuit-cutting strategy compatible with the semiclassical Fourier Transform [32]. This will permit the split of the circuits into several smaller circuits but requires classical communication between them, reducing the system size to execute the algorithm. We developed preliminary implementations of some of these topics during the Hackathon, but a more careful study is still pending.

References

[1] "Github repository". https://github.com/jgidi/VFA-Schrodinger-like-equations.

[2] Andrew J. Daley, Immanuel Bloch, Christian Kokail, Stuart Flannigan, Natalie Pearson, Matthias Troyer, and Peter Zoller. "Practical quantum advantage in quantum simulation". Nature **607**, 667–676 (2022).

[3] R P Feynman. "Simulating physics with computers". Int. J. of Th. Phys. **21**, 467 (1982).

[4] S Lloyd. "Universal Quantum Simulators". Science **273**, 1073–1078 (1996).

[5] Daniel S Abrams and Seth Lloyd. "Simulation of Many-Body Fermi Systems on a Universal Quantum Computer". Phys. Rev. Lett. **79**, 2586–2589 (1997).

[6] Gerald D Mahan. "Many-particle physics". Springer Science & Business Media. (2013).

[7] Ivan Kassal, Stephen P. Jordan, Peter J. Love, Masoud Mohseni, and Alán Aspuru-Guzik. "Polynomial-time quantum algorithm for the simulation of chemical dynam-

ics". Proceedings of the National Academy of Sciences **105**, 18681–18686 (2008). arXiv:https://www.pnas.org/doi/pdf/10.1073/pnas.0808245105.

[8] C Zalka. "Simulating quantum systems on a quantum computer". Proc. R. Soc. Lond. A **454**, 313–322 (1999).

[9] Stephen Wiesner. "Simulations of many-body quantum systems by a quantum computer" (1996). arXiv:quant-ph/9603028.

[10] Ryan Babbush, Dominic W. Berry, Jarrod R. McClean, and Hartmut Neven. "Quantum simulation of chemistry with sublinear scaling in basis size". npj Quantum Information **5**, 92 (2019).

[11] Yuan Su, Dominic W. Berry, Nathan Wiebe, Nicholas Rubin, and Ryan Babbush. "Fault-tolerant quantum simulations of chemistry in first quantization". PRX Quantum **2**, 040332 (2021).

[12] Alain Delgado, Pablo A. M. Casares, Roberto dos Reis, Modjtaba Shokrian Zini, Roberto Campos, Norge Cruz-Hernández, Arne-Christian Voigt, Angus Lowe, Soran Jahangiri, M. A. Martin-Delgado, Jonathan E. Mueller, and Juan Miguel Arrazola. "Simulating key properties of lithium-ion batteries with a fault-tolerant quantum computer". Phys. Rev. A **106**, 032428 (2022).

[13] Modjtaba Shokrian Zini, Alain Delgado, Roberto dos Reis, Pablo Antonio Moreno Casares, Jonathan E. Mueller, Arne-Christian Voigt, and Juan Miguel Arrazola. "Quantum simulation of battery materials using ionic pseudopotentials". Quantum **7**, 1049 (2023).

[14] W. Kohn. "Nobel lecture: Electronic structure of matter—wave functions and density functionals". Rev. Mod. Phys. **71**, 1253–1266 (1999).

[15] Stepan Fomichev, Kasra Hejazi, Modjtaba Shokrian Zini, Matthew Kiser, Joana Fraxanet Morales, Pablo Antonio Moreno Casares, Alain Delgado, Joonsuk Huh, Arne-Christian Voigt, Jonathan E. Mueller, and Juan Miguel Arrazola. "Initial state preparation for quantum chemistry on quantum computers" (2024). arXiv:2310.18410.

[16] Jarrod R. McClean, Sergio Boixo, Vadim N. Smelyanskiy, Ryan Babbush, and Hartmut Neven. "Barren plateaus in quantum neural network training landscapes". Nature Communications **9**, 1–6 (2018).

[17] Dian Wu, Riccardo Rossi, Filippo Vicentini, Nikita Astrakhantsev, Federico Becca, Xiaodong Cao, Juan Carrasquilla, Francesco Ferrari, Antoine Georges, Mohamed Hibat-Allah, Masatoshi Imada, Andreas M. Läuchli, Guglielmo Mazzola, Antonio Mezzacapo, Andrew Millis, Javier Robledo Moreno, Titus Neupert, Yusuke Nomura, Jannes Nys, Olivier Parcollet, Rico Pohle, Imelda Romero, Michael Schmid, J. Maxwell Silvester, Sandro Sorella, Luca F. Tocchio, Lei Wang, Steven R. White, Alexander Wietek, Qi Yang, Yiqi Yang, Shiwei Zhang, and Giuseppe Carleo. "Variational benchmarks for quantum many-body problems" (2023). arXiv:2302.04919.

[18] Paula García-Molina, Javier Rodríguez-Mediavilla, and Juan José García-Ripoll. "Quantum fourier analysis for multivariate functions and applications to a class of schrödinger-type partial differential equations". Phys. Rev. A **105**, 012433 (2022).

[19] P. Jordan and E. Wigner. "Über das paulische Äquivalenzverbot". Zeitschrift für Physik **47**, 631–651 (1928).

[20] Oscar Higgott, Daochen Wang, and Stephen Brierley. "Variational Quantum Computation of Excited States". Quantum **3**, 156 (2019).

[21] Robert B. Griffiths and Chi-Sheng Niu. "Semiclassical fourier transform for quantum computation". Physical Review Letters **76**, 3228–3231 (1996).

[22] S. Parker and M. B. Plenio. "Efficient factorization with a single pure qubit and log$N$ mixed qubits". Phys. Rev. Lett. **85**, 3049–3052 (2000).

[23] J. Chiaverini, J. Britton, D. Leibfried, E. Knill, M. D. Barrett, R. B. Blakestad, W. M. Itano, J. D. Jost, C. Langer, R. Ozeri, T. Schaetz, and D. J. Wineland. "Implementation of the semiclassical quantum fourier transform in a scalable system". Science **308**, 997–1000 (2005). arXiv:https://www.science.org/doi/pdf/10.1126/science.1110335.

[24] Thomas Monz, Daniel Nigg, Esteban A. Martinez, Matthias F. Brandl, Philipp Schindler, Richard Rines, Shannon X. Wang, Isaac L. Chuang, and Rainer Blatt. "Realization of a scalable shor algorithm". Science **351**, 1068–1070 (2016). arXiv:https://www.science.org/doi/pdf/10.1126/science.aad9480.

[25] A. Yu. Kitaev. "Quantum measurements and the abelian stabilizer problem" (1995). arXiv:quant-ph/9511026.

[26] Abhinav Kandala, Antonio Mezzacapo, Kristan Temme, Maika Takita, Markus Brink, Jerry M Chow, and Jay M Gambetta. "Hardware-efficient variational quantum eigensolver for small molecules and quantum magnets". Nature **549**, 242 (2017).

[27] L Rodney. "One-dimensional hydrogen atom". Proc. R. Soc. Lond. A**472** (2016).

[28] Assa Auerbach. "Interacting Electrons and Quantum Magnetism". Springer. (1998).

[29] Maxwell Aifer and Evan Sheldon. "Elliptic curves in continuous-variable quantum systems" (2024). arXiv:2401.11579.

[30] Ulf Leonhardt. "Quantum-state tomography and discrete wigner function". Phys. Rev. Lett. **74**, 4101–4105 (1995).

[31] James Dborin, Fergus Barratt, Vinul Wimalaweera, Lewis Wright, and Andrew G Green. "Matrix product state pre-training for quantum machine learning". Quantum Science and Technology **7**, 035014 (2022).

[32] Tianyi Peng, Aram W. Harrow, Maris Ozols, and Xiaodi Wu. "Simulating large quantum circuits on a small quantum computer". Phys. Rev. Lett. **125**, 150504 (2020).